

Topological antiferromagnetic spintronics: Part of a collection of reviews on antiferromagnetic spintronicsLibor Šmejkal,^{1,2,3} Yuriy Mokrousov,⁴ Binghai Yan,⁵ and Allan H. MacDonald⁶¹*Institute of Physics, Academy of Sciences of the Czech Republic, Cukrovarnicka 10, 162 00 Praha 6 Czech Republic*²*Institut für Physik, Johannes Gutenberg Universität Mainz, D-55099 Mainz, Germany*³*Faculty of Mathematics and Physics, Charles University in Prague, Ke Karlovu 3, 121 16 Prague 2, Czech Republic*⁴*Peter Grünberg Institut and Institute for Advanced Simulation, Forschungszentrum Jülich and JARA, 52425 Jülich, Germany*⁵*Department of Condensed Matter Physics, Weizmann Institute of Science, 7610001 Rehovot, Israel*⁶*Department of Physics, University of Texas at Austin, Austin, Texas 78712-0264, USA*

(Dated: 5 June 2017)

The recent demonstrations of electrical manipulation and detection of antiferromagnetic spins have opened up a chapter in the spintronics story. In this article, we review the emerging research field that is exploring synergies between antiferromagnetic spintronics and topological structures in real and momentum space. Active topics include proposals to realize Majorana fermions in an antiferromagnetic topological superconductors, to control topological protection of Dirac points by manipulating antiferromagnetic order parameters, and to exploit the anomalous and topological Hall effects of zero net moment antiferromagnets. We explain the basic physics concepts behind these proposals, and discuss potential applications of topological antiferromagnetic spintronics.

Topologically protected states of matter are unusually robust because they cannot be destroyed by small changes in system parameters. This feature of topological states has suggested an appealing strategy to achieve useful quantum computation^{1,2}. In spintronics, topological states provide for strong spin-momentum locking³, high charge-current to spin-current conversion efficiency⁴⁻⁶, large electron mobilities and long spin diffusion lengths^{7,8}, strong magnetoresistance⁸, and efficient spin-filtering⁹. Materials exhibiting topologically protected Dirac or Weyl quasiparticles in their momentum-space bands, and those exhibiting topologically non-trivial real-space spin textures^{6,10}, have both inspired new energy-efficient spintronics concepts^{4,7,10-13}.

In a topological insulator (TI), time reversal symmetry enforces Dirac quasiparticle surface states with spin-momentum locking (see Fig.1(a)) and protection against backscattering³. The much higher efficiency of magnetization switching by a current induced spin-orbit torque (SOT) in a TI/magnetically doped TI (MTI) heterostructure^{4,14} than in a heavy-metal/ferromagnet (FM) bilayer is thought to be associated with spin-momentum locking, and is a paradigmatic example of the potential seen for topological materials in spintronics. (A full microscopic understanding of the underlying current-spin conversion mechanism is however still absent¹⁵.) Progress in understanding and exploiting topological insulators in spintronics has so far been limited by unintentional bulk doping in TIs, and by the decreased stability of TI surface states at elevated temperatures¹⁵. The practical utility of the topologically enhanced SOT has also been limited by the cryogenic temperatures at which known MTIs order^{4,14,16}.

A substantial rise in the critical temperature of a magnetic topological insulator (by a factor of 3 to 90 K) due to proximity coupling to adjacent antiferromagnet (AF) has recently been demonstrated in a heterostructure consisting of the metallic antiferromagnet CrSb sandwiched between two MTIs¹⁷. Increased SOT efficiency at heterojunctions between TIs and ferrimagnetic CoTb alloys containing antiferromagnetically coupled Co and Tb sublattices¹⁸ has also been reported. The later effect persists to room temperature, but with decreased efficiency enhancement¹⁵ at higher temperatures. Research on using antiferromagnetism to achieve a role for topological materials in spintronics is however still at an early stage and many ideas have so far only been addressed theoretically. The practical advantages of TIs over heavy-metal systems for spin-orbit torques, for example, are not yet established¹⁵. The forms of magnetism so far incorporated in magnetic TIs remain fragile because they are of interfacial^{17,19} or dilute-moment character¹⁴. Other new ideas, beyond simply making topological insulators magnetic, are emerging at a rapid pace. In this article we review topological antiferromagnetic spintronics, the emerging field that is exploring the interplay between transport, topological properties in either momentum space or real space, and antiferromagnetic order.

I. TOPOLOGICAL INSULATORS IN ANTIFERROMAGNETS AND MAJORANA FERMIONS

The roots of topological antiferromagnetic spintronics can be traced to studies of layered AFs of the SrMnBi₂ type, which were thought to feature quasi 2D massive Dirac quasiparticles around the Fermi level^{20,21}. These were associated with the observation of enhanced mobilities, similarly to those in graphene. Masuda *et al.*²² have demonstrated manipulation of the Dirac quasiparticle current and the quantum Hall effect in a EuMnBi₂ AF by an applied strong magnetic field, with the effect of the field mediated by Eu sublattices.

As pointed out by Mong *et al.*²³, TI phases are possible in antiferromagnets even though time-reversal symmetry \mathcal{T} is broken and are protected instead by $T_{\frac{1}{2}}\mathcal{T}$ where $T_{\frac{1}{2}}$ is a half magnetic unit cell translation operation, as we illustrate in Fig.1(a). The proposed low-temperature AF candidate, GdPtBi, has not yet been confirmed as a TI by angle resolved photoemission spectroscopy (ARPES), presumably due to imperfect crystal momentum resolution of the measurement²⁴. A path of research related to topological superconductivity has demonstrated signatures of the coexistence of a 2D TI, *i.e.* the quantum spin Hall effect (QSHE), and a superconducting state in hole-doped and electron-doped antiferromagnetic monolayers of FeSe²⁵. FeSe is the metallic building block of the iron-based high- T_C superconductors. Surprisingly, the combined effect of substrate strain, spin-orbit coupling, and electronic correlations was shown to induce band inversion and QSHE edge states²⁵. These can in turn lead to the realization of Majorana zero modes, superconducting quasiparticle states with real wavefunctions that prevents decoherence, providing one route for the realization of quantum computing^{2,26} with topological qubits. The antiferromagnetic TI in combination with superconductivity can allow for an alternative realization of the Fu-Kane Majorana fermion proposal²⁷, possibly at higher temperatures²⁵. Separately, QSHE states in an AF have also been predicted in honeycomb lattice systems²⁸.

II. TOPOLOGICAL SEMIMETAL ANTIFERROMAGNETS

Topological semimetal states arise when conduction and valence bands touch at discrete points, lines, or planes in a bulk Brillouin zone at energies close to the Fermi level. The low energy physics of topological semimetals is governed by effective Dirac or Weyl equations^{11,13,29}. 3D Dirac and Weyl quasiparticles in non-magnetic bulk systems have attracted attention because of reports of suppressed backscattering, measurements of exotic topological surface states,

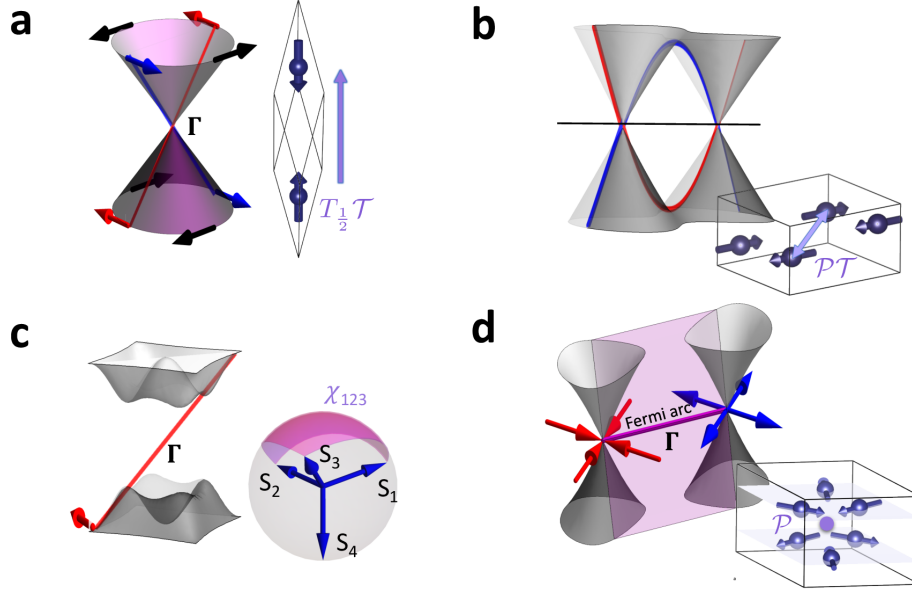


FIG. 1. (BOX:) Overview of the materials palette of topological antiferromagnetic spintronics: All panels show energy *vs.* crystal momentum band diagrams and magnetic structures. (a) Schematics of the spin-momentum locked surface-state Dirac quasiparticles in a TI. In the inset, we show the magnetic Gd sublattice of GdPtBi, an AF TI candidate. The magenta arrow marks the $T_{\frac{1}{2}}\mathcal{T}$ symmetry that protects a TI state in an AF. (b) Schematics of the bulk Dirac quasiparticles of an AF Dirac semimetal (DSM) that must be located along a high symmetry line in the BZ, and the magnetic structure of the AF DSM candidate CuMnAs. The \mathcal{PT} symmetry connects the magnetic Mn sublattices in pairs, and together with additional crystalline symmetry protects the DSM state as we explain in Fig.2(b). (c) Massive Dirac quasiparticles and QAHE edge states (red dispersion). A quantized Hall conductivity can be produced by the spin-chirality, $\chi_{ijk} = \hat{S}_i \cdot (\hat{S}_j \times \hat{S}_k)$, of a non-coplanar spin texture. The quantized topological Hall effect (QTHE) in a non-coplanar insulating AF gives rise to quantized edge states as in the QAHE, as we explain in the text. For the sake of simplicity, the non-coplanar spins of the antiferromagnetic QTHE candidate $K_{0.5}\text{RhO}_2$ are translated to a common origin. (d) Weyl points act as sources and drains of Berry curvature (blue and red arrows). In a centrosymmetric WSM, the topological charges are distributed antisymmetrically around the Γ point in the BZ. The noncollinear magnetic sublattice of antiferromagnetic Mn_3Ge forms kagome planes and has inversion symmetry \mathcal{P} . The pseudorelativistic linear band crossings in the left panels are found in the edge/surface states, whereas those in the right panels are realized in the bulk. The TI and DSM states (the two upper panels) cannot be realized in systems with ferromagnetic order, but are possible in antiferromagnets. In contrast, the QAHE/QTHE and WSM states (the two lower panels) are expected in both FMs and AFs, and can be formally obtained by breaking symmetries of the phases depicted in the two upper panels.

and interest in unique topological responses such as dissipationless axial currents.^{8,11,30} These properties are thought to be responsible for experimental observations of chiral magnetotransport^{12,31}, and strong magnetoresistance^{32,33}, although the topological origin of these phenomena is not yet firmly established⁸. For instance, the strong magnetoresistance in WTe_2 semimetals was originally explained on the basis on the carrier compensation in the tiny electron-hole pockets at the Fermi level³⁴, and only later linked to the presence of Weyl fermions³³.

A. Topological metal-insulator transitions in 3D Dirac semimetal antiferromagnets

In a system with time reversal \mathcal{T} and spatial inversion \mathcal{P} symmetries, the electronic bands are doubly degenerate resulting in a low energy Dirac Hamiltonian, $\mathcal{H}_D(\mathbf{k})$. In its simplest form^{11,13,29}:

$$\mathcal{H}_D(\mathbf{k}) = \begin{pmatrix} \hbar v_F \mathbf{k} \cdot \boldsymbol{\sigma} & m \\ m & -\hbar v_F \mathbf{k} \cdot \boldsymbol{\sigma} \end{pmatrix}, \quad (1)$$

where $\boldsymbol{\sigma}$ is the vector of Pauli matrices, v_F is the Fermi velocity, $\mathbf{k} = \mathbf{q} - \mathbf{q}_0$ is the crystal momentum measured from the Dirac point at \mathbf{q}_0 , and m is the mass (in units of energy). The corresponding energy dispersion reads $E_{\mathbf{k}} = \pm \hbar v_F \sqrt{k_x^2 + k_y^2 + k_z^2 + (\frac{m}{\hbar v_F})^2}$. The mass can vanish only when turned-off by a crystalline symmetry, and in

this case $\mathcal{H}_D(\mathbf{k})$ describes the four-fold degenerate band touching^{11,13} of a 3D Dirac semimetal (DSM) illustrated schematically in Fig.1(b). In a 3D DSM, the topological invariants and nontrivial surface states can be linked to the crystalline symmetry protecting the degeneracy^{35,36}.

The 3D DSM state is not possible in FMs because \mathcal{T} -symmetry breaking prevents double band degeneracy. On the other hand, a topological crystalline 3D Dirac semimetal was predicted in an AF, namely in the orthorhombic phase of CuMnAs^{37,38}. Here \mathcal{P} and \mathcal{T} symmetries are absent separately, but the combined effective \mathcal{PT} symmetry ensures double band degeneracy over the whole Brillouin zone. The DSM is in this case protected by \mathcal{PT} symmetry together with an additional crystalline non-symmorphic symmetry, as we explain in Fig. 2. The orthorhombic CuMnAs AF provides an attractive *hydrogen atom* for magnetic DSMs induced by the band inversion, since only a single pair of Dirac points appears near the Fermi level of the *ab initio* band structure. Electron filling enforced semimetals with a single Dirac cone are also a possibility as indicated theoretically in two dimensional model AFs³⁹.

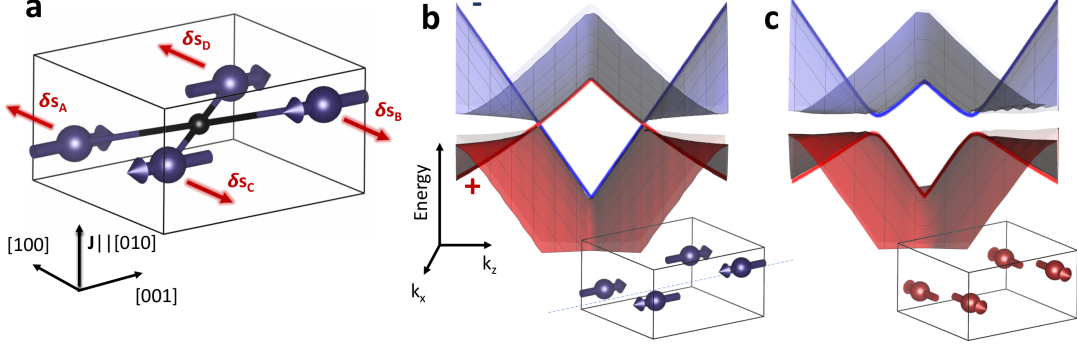


FIG. 2. (BOX:) **Topological metal-insulator transition in the antiferromagnetic DSM CuMnAs.** (a) The crystal and magnetic structure of the orthorhombic CuMnAs breaks time reversal and spatial inversion symmetry but preserves the combination \mathcal{PT} which connects the $A - B$ and $C - D$ Mn sublattices (Cu and As atoms are omitted for brevity). In the presence of an electrical current, owing to the \mathcal{PT} symmetry, a non-equilibrium staggered spin-polarization, $\delta\mathbf{s}$, is generated that can reorient the antiferromagnetic moments. (b) For a Néel vector along the $[001]$ axis, the crystal has a screw rotation symmetry \mathcal{S}_z which transforms the atom A into the atom C by a π -rotation along the z -axis followed by a $(\frac{1}{2}, 0, \frac{1}{2})$ -unit cell translation. \mathcal{S}_z prevents hybridization of doubly degenerate bands that have opposite eigenvalues of \mathcal{S}_z distinguished by ”+” and ”-” labels, and protects the DSM phase, as seen in the *ab initio* band structure. (c) For the $[100]$ orientation of the Néel vector, the \mathcal{S}_z symmetry is broken and the Dirac fermions acquire a mass giving rise to a semiconducting phase. This Néel vector reorientation controlled transition is referred to as the topological metal-insulator transition and can lead to extremely large anisotropic magnetoresistance.

Novel effects have been predicted in topological DSM AFs that are based on the possibility of controlling topological states by controlling only Néel vector orientation, not the presence or absence of antiferromagnetic order, and this can be accomplished using current-induced spin-orbit torques. The latter effect, discussed in detail by Železny *et al.* in this focused issue, has been experimentally demonstrated in CuMnAs⁴⁰. The coexistence of Dirac fermions and spin-orbit torques in CuMnAs implies a new phase transition mechanism, referred to as the topological metal-insulator transition (MIT)³⁸. The origin of the effect is in Fermi surface topology that is sensitive to the changes in the magnetic symmetry upon reorienting the Néel vector, as explained in Fig. 2. The transport counterpart of the topological MIT is topological anisotropic magnetoresistance (AMR), which in principle can reach extremely large values³⁸. The topological AMR can be understood as a limiting case of the crystalline AMR. The effect is different in origin and presumably more favorable for spintronics than the MIT observed in the pyrochlore iridate family which is driven by combined correlation and external field effects⁴¹, or the extreme magnetoresistance observed in the AF topological metal candidate NdSb⁴².

An antiferromagnetic Dirac nodal line semimetal has also been proposed³⁸. Here the band touching lines are protected by off-centered mirror plane symmetries and lead to distinct physical properties such as drum head surface states. Since the nodal-lines were observed several eV deep in the *ab initio* Fermi sea of tetragonal CuMnAs, the search is still on for more favorable candidate AF materials featuring nodal lines closer to the Fermi level.

B. Weyl fermions in antiferromagnets

When \mathcal{P} or \mathcal{T} symmetry, or both, is broken and the double band degeneracy is lifted, the touching points of two non-degenerate bands can form a 3D Weyl semimetal (WSM), see Fig.1(d). Fermi states in a WSM are described by

the Weyl Hamiltonian^{11,13}:

$$\mathcal{H}(\mathbf{k}) = \pm \hbar v_F \mathbf{k} \cdot \boldsymbol{\sigma}. \quad (2)$$

Weyl points act as monopoles sources of Berry curvature flux and generate a topological charge defined by:

$$\mathcal{C} = \frac{1}{2\pi} \int_{\delta S} d^2 k \mathbf{n} \cdot \langle \partial_{\mathbf{k}} u_{\mathbf{k}} | \times | \partial_{\mathbf{k}} u_{\mathbf{k}} \rangle = \pm 1. \quad (3)$$

Here δS is a small sphere surrounding the Weyl point with the surface normal vector \mathbf{n} and $\Omega_{\mathbf{k}} = \langle \partial_{\mathbf{k}} u_{\mathbf{k}} | \times | \partial_{\mathbf{k}} u_{\mathbf{k}} \rangle$ is the momentum space Berry curvature, which can be viewed as a fictitious magnetic field⁴³. In the vicinity of the Weyl point the Berry curvature takes the monopole form, $\Omega_{\mathbf{k}} = \pm \mathbf{k}/(2k^3)$. Weyl points always come in pairs with opposite topological charges and do not rely on any specific symmetry protection. The only way to remove them is to annihilate two Weyl points with opposite topological charges. This is in contrast to the DSM case in which gaps can open also due to the hybridization among the degenerate band partners when symmetries are weakly broken, as we explained in the previous section. The 3D nature of the Weyl point is crucial here since the corresponding Weyl equation uses all three Pauli matrices. Consequently, any small perturbation, that is in general expressed as a linear combination of Pauli matrices that form the basis of the 2×2 Hilbert space, just shifts but does not gap the Weyl point. (For example, for a perturbation of a form $m\sigma_z$, the dispersion is renormalized as $E_{\mathbf{k}} = \pm \hbar v_F \sqrt{k_x^2 + k_y^2 + (k_z + \frac{m}{\hbar v_F})^2}$.)

The initial prediction of the WSM by Wan et al⁴⁴ was for pyrochlore AFs. Subsequently, a Weyl metal state was predicted in the chiral non-collinear centrosymmetric AF Mn_3Ge (see Fig.1(c)), a metallic system in which trivial Fermi surface pockets are also present⁴⁵. Figs.3(a,b) illustrates the density of states weighted by the surface contribution which exhibits the typical Fermi arc features (see also Fig.1(d)), open surface state constant energy surfaces that connect the bulk projections of Weyl points, as found in *ab initio* calculations. We note that Weyl semimetal states can be also realized in the paramagnetic and AF phase of GdPtBi ^{12,31} by applying a magnetic field and, in contrast to DSMs, WSMs can in principle exist also in FMs⁴⁶.

The presence of Weyl points in the pyrochlore AF $\text{Eu}_2\text{Ir}_2\text{O}_7$ ⁴⁷ was inferred from optical experiments. However, a direct spectroscopic identification (*e.g.* by ARPES) of these Weyl AFs has yet to be made^{29,48}. The YbMnBi_2 AF was originally proposed to be WSM based on the ARPES identification of the bandcrossings consistent with the *ab initio* bandstructure calculated for the canted AF moments⁴⁹, later supported by an optical study⁵⁰. However, recent magnetotransport⁵¹ and optical conductivity⁵² measurements in the YbMnBi_2 AF were shown to be rather consistent with the Dirac quasiparticles²⁹. The Mn_3Ge AF was shown to host a large anomalous Hall effect (AHE) whose origin is discussed in the next section.

III. HALL EFFECTS IN NONCOLLINEAR TOPOLOGICAL ANTIFERROMAGNETS

Until recently the AHE was viewed as a combined consequence of the time reversal symmetry breaking in a ferromagnet and spin-orbit coupling⁵⁵. In the case of collinear AFs, either $T_{\frac{1}{2}}\mathcal{T}$ symmetry or \mathcal{PT} symmetry forces the Hall conductivity to vanish. Recent *ab initio* calculations^{56,57} inspired by earlier theoretical work^{58,59,60}, have however shown that time-reversal symmetry breaking by AF order can yield a finite Hall response in some non-collinear AFs, even those with zero net magnetization and even in the absence of spin-orbit coupling. The time reversal symmetry breaking is manifested by a nonzero Berry curvature, as we show in Fig.3(d). The intrinsic contribution to the Hall conductivity depends only on the band structure of the perfect crystal and can be calculated from linear response theory⁵⁵:

$$\sigma_{xz} = \frac{e^2}{\hbar} \sum_n \int_{\text{BZ}} \frac{d^3 k}{(2\pi)^3} f(\mathbf{k}) \Omega_y^n(\mathbf{k}), \quad (4)$$

where $\Omega_y^n(\mathbf{k})$ is the y -component of the fictitious magnetic field, or the Berry curvature (cf. Eq.(3)), and n is the band index.

A. The Anomalous Hall effect in antiferromagnets

In the simplest toy model of a WSM (with a two Weyl points in the vicinity of the Fermi level), the AHE conductivity can be calculated by integrating the quantized two-dimensional Hall conductivities of momentum-planes that are

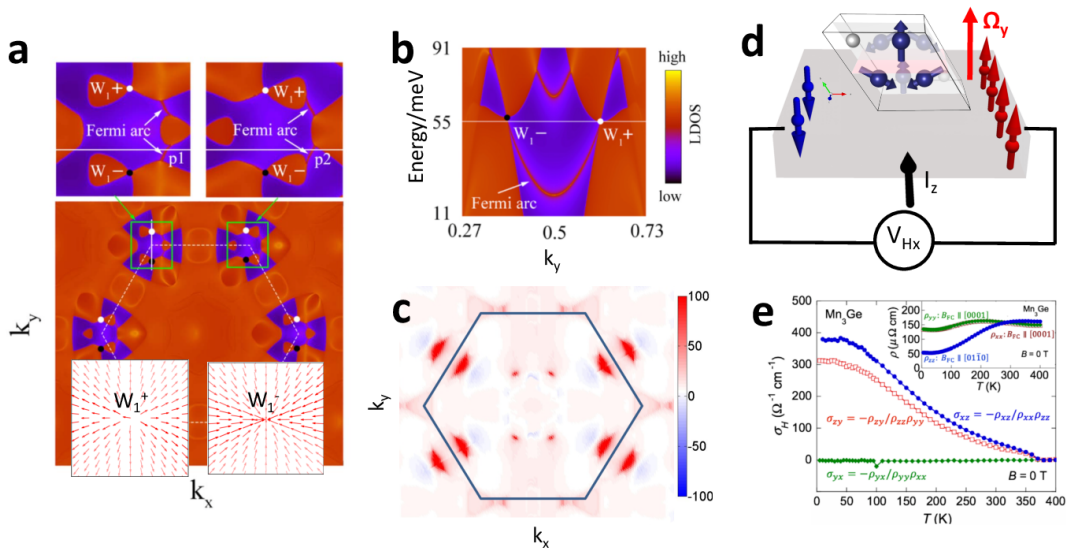


FIG. 3. **Weyl fermions and Hall effects in noncollinear AFs.** (a) The density of states weighted by the surface contribution calculation reveals the Fermi surface with visible Fermi arcs. The Berry curvature vector field around the two Weyl points with opposite charges is plotted in two lower insets. (b) Weyl points in Mn₃Ge close to the Fermi level are connected by surface state Fermi arcs as calculated *ab initio*. (c) The largest contribution to the intrinsic AHE originates from avoided crossing lines where the fictitious magnetic field, i.e. the Berry curvature, takes the largest value. (d) The concept of magnetic memory bits in a non-collinear AF Mn₃Ge. The measured large anomalous Hall effect at the room temperature originates in breaking the effective time reversal symmetry combining time reversal and mirror plane symmetries by the non-collinear magnetic order, as shown in the inset on the magnetic structure of Mn₃Ge. The magnetic information can be stored in the orientation of the non-collinear AF order since a reorientation by, e.g., a weak magnetic field $\mathbf{B}_{[010]}$ can flip the sign of the anomalous Hall voltage V_H (and the corresponding conductivity σ_{xz}) for the applied current along the [001] direction. Temperature dependence of (e) the AHE conductivity in Mn₃Ge. The Figs.(a-b, and e) were adapted from^{45,54}.

perpendicular to the line connecting Weyl points to obtain,

$$\sigma_{xy} = \frac{e^2}{h} \frac{\Delta k_W}{2\pi}, \quad (5)$$

where Δk_W is the distance between Weyl points⁶¹. The AHE was recently observed in the hexagonal noncollinear AFs Mn₃Sn and Mn₃Ge^{54,62,63}, which have Weyl points close to the Fermi level. However, *ab initio* calculations of the intrinsic AHE in Mn₃Ge, which predict a magnitude consistent with experiment (see Fig.3(e)), reveal that the dominant contribution to the AHE comes instead from localized avoided crossings in the band structure⁵³. This property is illustrated in Fig.3(c) by calculating crystal momentum projected contributions of the Berry curvature/conductivity $\sim \int_{k_z} dk_z \Omega_y(k_x, k_y, k_z)$. We also note that a large AHE was achieved in the collinear AF GdPtBi, by canting the staggered order⁶⁴.

The discovery of a large AHE Mn₃Ge, which is a metal but has a relatively small density-of-states at the Fermi level, inspires a search for the quantized and dissipationless limits of the anomalous transport in topological semiconducting/insulating AFs. A quantum anomalous Hall effect (QAHE) with quantized charged edge state channels was proposed for antiferromagnetic insulators^{65,66}. In a two-band 2D Chern insulator with Hamiltonian $\mathcal{H}_{\mathbf{k}} = \mathbf{d}(\mathbf{k}) \cdot \boldsymbol{\sigma}$, the 2D variant of Eq.(4) reads

$$\sigma_{xy} = \frac{e^2}{h} \frac{1}{4\pi} \sum_n \int_{\text{BZ}} dk_x dk_y \hat{\mathbf{d}} \cdot \left(\partial_{k_x} \hat{\mathbf{d}} \times \partial_{k_y} \hat{\mathbf{d}} \right), \quad (6)$$

where $\hat{\mathbf{d}}(\mathbf{k}) = \mathbf{d}(\mathbf{k})/|\mathbf{d}(\mathbf{k})|$. The integral is quantized and relates directly to the Chern number (c.f. Eq.(3)).

While the AHE arises from the Berry curvature in the momentum space, other important spintronic phenomena can be associated with Berry curvatures in different parameter spaces. For instance, the spin-orbit torque tensor is defined by the linear response relation $\mathbf{T} = \tau \mathbf{E}$, where $\mathbf{T} = \frac{d\mathbf{m}}{dt}$ is the SOT exerted on the magnetization \mathbf{m} in a magnet subject to an applied electric field \mathbf{E} . The intrinsic part of the SOT can be rewritten in terms of a mixed Berry curvature, $\Omega_{ij}^{\mathbf{m}\mathbf{k}} = \hat{\mathbf{e}}_i \cdot 2\text{Im} \sum_n \langle \partial_{\hat{\mathbf{m}}} u_{kn} | \partial_{k_j} u_{kn} \rangle$, where $\hat{\mathbf{e}}_i$ denotes the i th Cartesian unit vector and $\hat{\mathbf{m}}$ is a

unit vector in the direction of magnetization⁶⁷. A large SOT in a topologically nontrivial insulating FM has been associated with the existence of the monopoles of the mixed Berry curvature. These are termed mixed Weyl points as they correspond formally to a Weyl Hamiltonian $\mathcal{H}(\mathbf{k}, \hat{\mathbf{m}}) = \hbar v_F (k_x \sigma_x + k_y \sigma_y) + v_\theta \theta \sigma_z$ in the mixed momentum-magnetization space⁶⁷. (Here θ is the azimuthal angle of the magnetization.) The recent discovery of the SOT and the prediction of the DSM in antiferromagnetic CuMnAs motivates a search for analogous dissipationless (pronounced) SOTs in insulating AFs. Finally, we note that spintronics based on insulating AFs may utilize the concept of Weyl magnons (a boson analog of Weyl fermions), that has been proposed in pyrochlore AFs⁶⁸.

B. Topological Hall effect in antiferromagnets

Real-space order parameter textures can be induced in AFs, and their presence can be detected by the so-called topological Hall effect. In this phenomenon, the role of the spin-orbit coupling is substituted by the chirality of the spin texture (see inset in Fig.1(c)), $\chi_{ijk} = \hat{S}_i \cdot (\hat{S}_j \times \hat{S}_k)$. (Note that the spin-chirality vanishes in coplanar AFs like Mn₃Ge.) The effect of the corresponding fictitious magnetic field, $\hat{\mathbf{m}} \cdot (\partial_x \hat{\mathbf{m}} \times \partial_y \hat{\mathbf{m}})$, on the Bloch electrons generates a Hall response. The topological Hall effect can be experimentally distinguished from the AHE by, e.g., analyzing the disorder dependence⁶⁹. However, the distinction at surfaces might be difficult as was pointed out in studies of monolayer Fe deposited on an Ir(001) surface⁷⁰.

The Hall effect associated with the spin-chirality was initially reported in antiferromagnetic pyrochlore iridates⁷¹ and later in MnSi chiral antiferromagnetic alloys^{72,73}. We note that the term "topological" used to label the effect does not imply in this case a correspondence to a topological invariant. This is in contrast to skyrmions discussed in more detail in the following section. A skyrmion spin texture carries an integer topological charge which is accompanied with a topological Hall effect. In this case, the term topological refers to the association of the Hall response to a topological invariant. Another example of such a correspondence is the quantum topological Hall effect which was proposed for the non-coplanar AF K_{0.5}RhO₂⁷⁴, as we show schematically in Fig.1(d). Unlike skyrmions, here the topological charge occurs in the momentum space, i.e., is obtained from Eq.(4) giving an integer value.

Finally, topological systems were predicted also as promising generators of the spin Hall effect (SHE). The WSM TaAs was predicted to host a large spin Hall angle arising mainly from the nodal line anticrossing features⁷⁵. Similarly, a topological SHE was predicted for skyrmions⁷⁶ where the spin Hall response occurs even in the absence of the spin-orbit coupling, in analogy with the above topological (charge) Hall effect. Recently, it was theoretically proposed that the SHE can occur also due to the breaking of the spin rotational symmetry in non-collinear AFs without the need for either the spin-orbit coupling or the spin-chirality⁷⁷.

In noncollinear AFs, other "topological" phenomena might arise, such as the topological orbital magnetism in Fe/Ir(001), Mn/Cu(111) or in the γ -phase of FeMn alloy^{70,78,79}. The effect is rooted in the spin-chirality of non-coplanar spin textures, exists also without the spin-orbit coupling, and does not have to be associated with an integer topological invariant⁷⁹. Novel functionalities can be envisaged by controlling the topological orbital magnetism via spin-torque manipulation of the spin textures or via the spin-orbit coupling⁷⁹.

IV. ANTIFERROMAGNETIC SKYRMIONS

As noted above, position-dependent magnetization textures can also be topologically non-trivial. Skyrmions are noncollinear magnetization textures in which the spin quantization axis changes continuously over length scales that vary from a few nm to a few μm . For two-dimensional systems, the winding number,

$$Q^{(j)} = \frac{1}{4\pi} \int dx dy \hat{\mathbf{m}}^{(j)} \cdot (\partial_x \hat{\mathbf{m}}^{(j)} \times \partial_y \hat{\mathbf{m}}^{(j)}), \quad (7)$$

of a magnetization texture measures the number of times the sphere of magnetization directions is covered upon integrating over space and must take on integer values^{10,82}. Here $\hat{\mathbf{m}} = \mathbf{m}(x, y, z)$ is the normalised magnetization field in the real space and $\hat{\mathbf{m}} \cdot (\partial_x \hat{\mathbf{m}} \times \partial_y \hat{\mathbf{m}})$ is the fictitious emergent magnetic field. The antiferromagnetic skyrmion can be visualized as two interpenetrating ferromagnetic skyrmions, where the index $(j) = (1, 2)$ labels the two antiferromagnetic sublattices, as shown in Fig.4(a). Microscopically, the skyrmionic magnetization modulation is caused by the Dzyaloshinskii-Moriya interaction (DMI) of non-centrosymmetric crystals. Whereas ferromagnetic skyrmions are often generated by interfacial DMIs, antiferromagnetic skyrmions are expected to be more abundant in crystals with bulk DMI⁸³.

By comparing to Eq.(3), and (6) we see that the winding number Q topologically protects skyrmion textures in real space, just as Weyl points and the QAHE state are protected in momentum space. The observed energy barrier

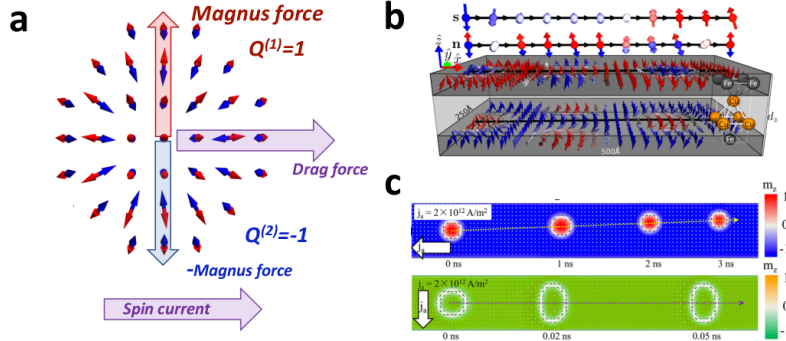


FIG. 4. **Antiferromagnetic skyrmions.** (a) An antiferromagnetic skyrmion can be viewed as consisting of two antiferromagnetically coupled ferromagnetic skyrmions. For the sake of clarity, we draw the two opposite magnetic moments in the antiferromagnetic unit cell as coinciding and their moments as perfectly compensated. Note that the structure of the skyrmion is analogous to the momentum-space Berry curvature shown in the inset of Fig.3(a). (b) A synthetic antiferromagnetic skyrmion in a Fe-Cu-Fe trilayer. (c) Micromagnetic simulation of ferromagnetic (upper panel) and antiferromagnetic (lower panel) skyrmion motion driven by a SOT. The ferromagnetic skyrmion is deflected by the Magnus force, while the antiferromagnetic skyrmion can move in a straight line due to mutual compensation between Magnus forces from the two magnetic sublattices, as schematically shown in panel (a). Panels (b)-(c) are adapted from Refs. 80 and 81.

for skyrmion annihilation in discrete magnetic skyrmions is of the order of ~ 0.1 eV⁸⁴. Because this barrier is finite, skyrmion stability in experimental systems relies in part on other physical limitations, (*e.g.* a combined effect of spin rotation and skyrmion diameter shrinking) rather than from topological protection itself⁸⁴.

Skyrmions in non-centrosymmetric AFs were considered already some time ago⁸⁵ in various contexts, including in connection with high-temperature superconductivity⁸⁶. However, spintronics aspects of antiferromagnetic skyrmions, namely their manipulation by an electrical current, were discussed only recently^{81,87-89}. Micromagnetic simulations show that antiferromagnetic skyrmions move faster than ferromagnetic skyrmions, can be driven with lower current densities and, most importantly, move in straight lines, as illustrated in Fig. 4(c)^{81,87,88}. This important difference arises because the Magnus force which deflects ferromagnetic skyrmions has opposite sign for the two magnetic sublattices of an antiferromagnetic skyrmion, owing to the opposite topological numbers illustrated in Fig.4(a). AF skyrmions were recently studied in detail also in synthetic AFs (*e.g.* in a Fe|Cu|Fe trilayer) in which skyrmions in the two ferromagnetic layers are coupled antiferromagnetically^{80,90}, as shown in Fig. 4(b). The topological SHE was suggested as a probe to monitor the AF skyrmions, as well as to generate a spin current⁸⁰.

V. PERSPECTIVES

The past year has seen important progress in coupling topological phases of matter with AF order. The fortunate lattice constant match between the Cr-doped TI $(\text{Bi,Sb})_2\text{Te}_3$, and the high temperature AF CrSb (see Fig.5(a)) has been exploited to grow epitaxial interfaces between these materials. The resulting heterostructures exhibit strengthened order in the MTI¹⁷, enhancing topological effects in its electronic properties. CrSb/ $(\text{Bi,Sb})_2\text{Te}_3$ /CrSb trilayers exhibit cusps in the magnetoresistance, that presumably correspond to a topological phase transition of Dirac quasiparticles at the interfaces⁹². Separately, in studies of $\text{Bi}_2\text{Se}_3/\text{CoTb}$ heterostructures¹⁵, it was also shown that a SOT from a TI can manipulate the AF-coupled sublattices in an adjacent ferrimagnet. Further progress in which perfectly compensated antiferromagnetic materials are employed can enable the advantages of AF spintronics, discussed throughout this issue, to be realized more fully. AF FeSe monolayers will likely be tested for the realization of Majorana-based topological quantum qubits. Making a p-n junction in a single layer of FeSe by gating can generate two regions - one superconducting and one with a QSHE²⁶. Coupling this system to two FM electrodes from both sides would lead to localization of Majorana modes at the interface as illustrated in Fig.5(b). This two level state can function as a quantum bit which can nonlocally encode information and is robust against decoherence due to the real wavefunction of the Majorana modes².

In this brief review, we have focused on direct synergies between antiferromagnetic and topological properties in crystal momentum and real spaces. Novel magnetic topological phases of matter were predicted only very recently and in many cases remain experimentally elusive, *e.g.* AF TIs, DSMs, and WSMs, QAHE states, and skyrmions. When realized, these topological antiferromagnet states can lead not only to more stable topological nanospintronics devices, but also to unprecedented functionalities relying on the unique AF symmetries and the possibility of tuning them by

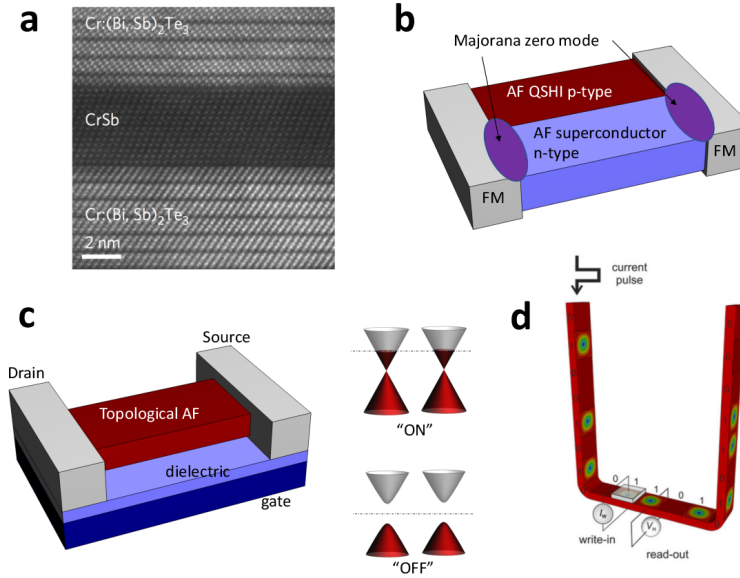


FIG. 5. **Topological spintronics based on antiferromagnets.** (a) Example of a possible building block for topological AF spintronics in heterostructures: an epitaxially matched interface between AF CrSb and a Cr-doped MTI. (b) A Majorana qubits in an AF FeSe monolayer. (c) A concept of a topological transistor explained in the text. (d) The skyrmion racetrack memory concept. Magnetic information is stored in a topological charge Q instead of the magnetization of the magnetic domain. "1" encodes the skyrmion with $Q=1$, while "0" corresponds to a uniform domain with $Q=0$. Spin transfer torque shifts the register. Bits read by the topological Hall effect and written by nucleating or deleting the skyrmion. Panels (a), and (d) are adapted from Refs. 17 and 91.

external means by coupling to the AF order. Fast topological memories, in which states are written by the topological SOT in an AF TI, or an AF DSM^{38,67,93}, and read out via the large magnetoresistance effects associated with band gap tuning^{38,94,95}, are among anticipated applications. Another possibility is opened by exploiting topological phase transitions, as we have explained for the CuMnAs Dirac AF in the Fig.2. Here one can foresee the possibility of a topological transistor operating at high frequencies and low current densities (see Fig.5(c))⁹⁶. In contrast to the related proposal in crystalline topological insulators⁹⁷, one can achieve highly mobile bulk Dirac quasiparticle current (present in the "ON" state) controllable by gating or by ultrafast SOT. We note that many of the novel effects we have discussed follow directly from antiferromagnetic symmetries and cannot be realized in FMs, for instance (i) magnetism combined with the QSHE, and superconductivity, and (ii) magnetism combined with Dirac semimetal phase. The conditions for a good Dirac quasiparticle in AF spintronics were discussed recently¹³.

The sign and magnitude of the AHE in Mn₃Ge depends on the noncollinear spin texture orientation. This together with the demonstration of the possibility of manipulating the noncollinear spin texture by a spin-torque⁹⁸ can allow for memory devices in noncollinear AFs, with the electrical readout via the AHE, as illustrated in Fig.3(d). Moreover, optical counterparts of the dc AHE should be present in non-collinear AFs⁹⁹, opening the prospect for optical detection of topological effects and of antiferromagnetic opto-spintronic devices.

The nontrivial topologies of magnetization texture might also find applications. The skyrmion might represent the smallest micromagnetic configuration for storing information before going into truly quantum mechanical single spin qubits⁶. For instance, in the skyrmionic racetrack memory, as shown in Fig. 5(d), the magnetic information is stored in skyrmions instead of magnetic domains separated by domain walls¹⁰. Skyrmions can be driven by the SOT at low current densities and have advantages over domain walls especially in the curved parts of the race track thanks to their stability.

After almost a half century of research we have discovered many manifestations of topology playing a role in materials physics, from spin liquids, to Quantum Hall effects, to the theory of dislocations¹⁰⁰ and beyond. In this article, we have highlighted a newly emerging field, topological antiferromagnetic spintronics. Beyond providing an interesting new context in which to identify and understand the physical consequences of topological properties in momentum-space bands or real-space textures, topological antiferromagnetic spintronics suggests the tantalizing possibility of converting important fundamental advances to truly valuable new applications of quantum materials.

Acknowledgement LŠ acknowledges support from the Grant Agency of the Charles University, no. 280815. Access to computing and storage facilities owned by parties and projects contributing to the National Grid Infrastructure

MetaCentrum provided under the program Projects of Large Research, Development, and Innovations Infrastructures (CESNET LM2015042) is greatly appreciated. YM acknowledges funding from the German Research Foundation (Deutsche Forschungsgemeinschaft, Grant No. MO 1731/5-1). B.Y. acknowledges support of the Ruth and Herman Albert Scholars Program for New Scientists in Weizmann Institute of Science, Israel. AHM was supported by SHINES, an Energy Frontier Research Center funded by the U.S. Department of Energy, Office of Science, Basic Energy Sciences under Award #SC0012670, and by Welch Foundation grant TBF1473.

REFERENCES

- ¹S. D. Sarma, M. Freedman, and C. Nayak, “Majorana Zero Modes and Topological Quantum Computation,” *Nat. Publ. Gr.* (2015), 10.1038/npjqi.2015.1, arXiv:1501.02813.
- ²C. W. J. Beenakker and L. Kouwenhoven, “A road to reality with topological superconductors,” *Nat. Phys.* **12**, 618–621 (2016), arXiv:1606.09439v1.
- ³M. Z. Hasan and C. Kane, “Colloquium: Topological insulators,” *Rev. Mod. Phys.* **82**, 3045–3067 (2010).
- ⁴Y. Fan and K. L. Wang, “Spintronics Based on Topological Insulators,” *SPIN* **06**, 1640001 (2016).
- ⁵H. Wang, J. Kally, J. S. Lee, T. Liu, H. Chang, D. R. Hickey, K. A. Mkhoyan, M. Wu, A. Richardella, and N. Samarth, “Surface-State-Dominated Spin-Charge Current Conversion in Topological-Insulator/Ferromagnetic-Insulator Heterostructures,” *Phys. Rev. Lett.* **117**, 076601 (2016).
- ⁶A. Soumyanarayanan, N. Reyren, A. Fert, and C. Panagopoulos, “Spin-Orbit Coupling Induced Emergent Phenomena at Surfaces and Interfaces,” *Nature* **539**, 509–517 (2016), arXiv:1611.09521.
- ⁷D. A. Pesin and A. H. MacDonald, “Spintronics and pseudospintronics in graphene and topological insulators,” *Nat. Mater.* **11**, 409–416 (2012).
- ⁸T. Liang, Q. Gibson, M. N. Ali, M. Liu, R. J. Cava, and N. P. Ong, “Ultrahigh mobility and giant magnetoresistance in the Dirac semimetal Cd₃As₂,” *Nat. Mater.* **14**, 280–284 (2014).
- ⁹J. Wu, J. Liu, and X. J. Liu, “Topological spin texture in a quantum anomalous hall insulator,” *Phys. Rev. Lett.* **113**, 136403 (2014), arXiv:1401.0415.
- ¹⁰A. Fert, V. Cros, and J. Sampaio, “Skyrmions on the track,” *Nat. Nanotechnol.* **8**, 152–156 (2013).
- ¹¹A. A. Burkov, “Topological semimetals,” *Nat. Mater.* **15**, 1145–1148 (2016), arXiv:1610.07866.
- ¹²C. Felser and B. Yan, “Weyl semimetals: Magnetically induced,” *Nat. Mater.* **15**, 1149–1150 (2016).
- ¹³L. Šmejkal, T. Jungwirth, and J. Sinova, “Route Towards Dirac and Weyl Antiferromagnetic Spintronics,” *Phys. Stat. Sol.* (2017), 10.1002/pssr.201700044, arXiv:1702.07788.
- ¹⁴Y. Fan, P. Upadhyaya, X. Kou, M. Lang, S. Takei, Z. Wang, J. Tang, L. He, L.-T. Chang, M. Montazeri, G. Yu, W. Jiang, T. Nie, R. N. Schwartz, Y. Tserkovnyak, and K. L. Wang, “Magnetization switching through giant spin-orbit torque in a magnetically doped topological insulator heterostructure,” *Nat. Mater.* **13**, 699–704 (2014).
- ¹⁵J. Han, A. Richardella, S. Siddiqui, J. Finley, N. Samarth, and L. Liu, “Room temperature spin-orbit torque switching induced by a topological insulator,” (2017), arXiv:1703.07470.
- ¹⁶A recent report¹⁹ of interfacial ferromagnetism persisting to room temperature at a insulating ferromagnet (EuS)/TI heterostructure is promising in this respect.
- ¹⁷Q. L. He, X. Kou, A. J. Grutter, G. Yin, L. Pan, X. Che, Y. Liu, T. Nie, B. Zhang, S. M. Disseler, B. J. Kirby, W. Ratcliff II, Q. Shao, K. Murata, X. Zhu, G. Yu, Y. Fan, M. Montazeri, X. Han, J. A. Borchers, and K. L. Wang, “Tailoring exchange couplings in magnetic topological-insulator/antiferromagnet heterostructures,” *Nat. Mater.* **16**, 94–100 (2016).
- ¹⁸J. Finley and L. Liu, “Spin-Orbit-Torque Efficiency in Compensated Ferrimagnetic Cobalt-Terbium Alloys,” *Phys. Rev. Appl.* **6**, 054001 (2016).
- ¹⁹F. Katmis, V. Lauter, F. S. Nogueira, B. A. Assaf, M. E. Jamer, P. Wei, B. Satpati, J. W. Freeland, I. Eremin, D. Heiman, P. Jarillo-Herrero, and J. S. Moodera, “A high-temperature ferromagnetic topological insulating phase by proximity coupling,” *Nature* **533**, 513–516 (2016).
- ²⁰J. Park, G. Lee, F. Wolff-Fabris, Y. Y. Koh, M. J. Eom, Y. K. Kim, M. A. Farhan, Y. J. Jo, C. Kim, J. H. Shim, and J. S. Kim, “Anisotropic Dirac Fermions in a Bi Square Net of SrMnBi₂,” *Phys. Rev. Lett.* **107**, 126402 (2011), arXiv:1104.5138.
- ²¹K. Wang, D. Graf, H. Lei, S. W. Tozer, and C. Petrovic, “Quantum transport of two-dimensional Dirac fermions in SrMnBi₂,” *Phys. Rev. B - Condens. Matter Mater. Phys.* **84**, 220401(R) (2011), arXiv:1204.1049v1.
- ²²H. Masuda, H. Sakai, M. Tokunaga, Y. Yamasaki, A. Miyake, J. Shiogai, S. Nakamura, S. Awaji, A. Tsukazaki, H. Nakao, Y. Murakami, T.-h. Arima, Y. Tokura, and S. Ishiwata, “Quantum Hall effect in a bulk antiferromagnet EuMnBi₂ with magnetically confined two-dimensional Dirac fermions,” *Sci. Adv.* **2**, e1501117 (2016).
- ²³R. S. K. Mong, A. M. Essin, and J. E. Moore, “Antiferromagnetic topological insulators,” *Phys. Rev. B* **81**, 245209 (2010), arXiv:1004.1403.

- ²⁴C. Liu, Y. Lee, T. Kondo, E. D. Mun, M. Caudle, B. N. Harmon, S. L. Bud, P. C. Canfield, and A. Kaminski, “Metallic surface electronic state in half-Heusler compounds RPtBi (R = Lu, Dy, Gd),” **83**, 205133 (2011) (2011).
- ²⁵Z. F. Wang, H. Zhang, D. Liu, C. Liu, C. Tang, C. Song, Y. Zhong, J. Peng, F. Li, C. Nie, L. Wang, X. J. Zhou, X. Ma, Q. K. Xue, and F. Liu, “Topological edge states in a high-temperature superconductor FeSe/SrTiO₃(001) film,” *Nat. Mater.* **15**, 968 (2016).
- ²⁶W.-F. Tsai and H. Lin, “Topological insulators and superconductivity: The integrity of two sides,” *Nat. Mater.* (2016), 10.1038/nmat4700.
- ²⁷L. Fu and C. L. Kane, “Superconducting Proximity Effect and Majorana Fermions at the Surface of a Topological Insulator,” *Phys. Rev. Lett.* **100**, 096407 (2008).
- ²⁸C. Niu, J. P. Hanke, P. M. Buhl, G. Bihlmayer, D. Wortmann, S. Blügel, and Y. Mokrousov, “Quantum spin Hall effect and topological phase transitions in honeycomb antiferromagnets,” , 1–5 (2017), arXiv:1705.07035.
- ²⁹N. P. Armitage, E. J. Mele, and A. Vishwanath, “Weyl and Dirac Semimetals in Three Dimensional Solids ,” (2017), arXiv:1705.01111v1.
- ³⁰S. Jia, S.-Y. Xu, and M. Z. Hasan, “Weyl semimetals, Fermi arcs and chiral anomalies,” *Nat. Mater.* **15**, 1140–1144 (2016).
- ³¹M. Hirschberger, S. Kushwaha, Z. Wang, Q. Gibson, S. Liang, C. A. Belvin, B. A. Bernevig, R. J. Cava, and N. P. Ong, “The chiral anomaly and thermopower of Weyl fermions in the half-Heusler GdPtBi,” *Nat. Mater.* **15**, 1161–1165 (2016), arXiv:1602.07219.
- ³²M. N. Ali, J. Xiong, S. Flynn, J. Tao, Q. D. Gibson, L. M. Schoop, T. Liang, N. Haldolaarachchige, M. Hirschberger, N. P. Ong, and R. J. Cava, “Large, non-saturating magnetoresistance in WTe₂,” *Nature* **514**, 205–208 (2014), arXiv:1405.0973.
- ³³A. A. Soluyanov, D. Gresch, Z. Wang, Q. Wu, M. Troyer, X. Dai, and B. A. Bernevig, “Type-II Weyl semimetals,” *Nature* **527**, 495–498 (2015).
- ³⁴I. Pletikoscic, M. N. Ali, A. V. Fedorov, R. J. Cava, and T. Valla, “Electronic structure basis for the extraordinary magnetoresistance in WTe₂,” *Phys. Rev. Lett.* **113**, 216601 (2014), arXiv:1407.3576v1.
- ³⁵B.-j. Yang and N. Nagaosa, “Classification of stable three-dimensional Dirac semimetals with nontrivial topology,” *Nat. Commun.* **5**, 4898 (2014), arXiv:1404.0754v1.
- ³⁶M. Kargarian, M. Randeria, and Y.-M. Lu, “Are the surface Fermi arcs in Dirac semimetals topologically protected?” *Proc. Natl. Acad. Sci.* **113**, 8648–8652 (2016).
- ³⁷P. Tang, Q. Zhou, G. Xu, and S.-C. Zhang, “Dirac fermions in an antiferromagnetic semimetal,” *Nat. Phys.* **12**, 1100–1104 (2016).
- ³⁸L. Šmejkal, J. Železný, J. Sinova, and T. Jungwirth, “Electric Control of Dirac Quasiparticles by Spin-Orbit Torque in an Antiferromagnet,” *Phys. Rev. Lett.* **118**, 106402 (2017).
- ³⁹S. M. Young and B. J. Wieder, “Filling-enforced Magnetic Dirac Semimetals in Two Dimensions,” *Phys. Rev. Lett.* **118**, 186401 (2017), arXiv:1609.06738.
- ⁴⁰P. Wadley, B. Howells, J. Zelezny, C. Andrews, V. Hills, R. P. Campion, V. Novak, K. Olejnik, F. Maccherozzi, S. S. Dhesi, S. Y. Martin, T. Wagner, J. Wunderlich, F. Freimuth, Y. Mokrousov, J. Kunes, J. S. Chauhan, M. J. Grzybowski, A. W. Rushforth, K. W. Edmonds, B. L. Gallagher, and T. Jungwirth, “Electrical switching of an antiferromagnet,” *Science* **351**, 587–590 (2016).
- ⁴¹Z. Tian, Y. Kohama, T. Tomita, H. Ishizuka, T. H. Hsieh, J. J. Ishikawa, K. Kindo, L. Balents, and S. Nakatsuji, “Field-induced quantum metalinsulator transition in the pyrochlore iridate Nd₂Ir₂O₇,” *Nat. Phys.* **12**, 134 (2015).
- ⁴²N. Wakeham, E. D. Bauer, M. Neupane, and F. Ronning, “Large magnetoresistance in the antiferromagnetic semimetal NdSb,” *Phys. Rev. B - Condens. Matter Mater. Phys.* **93**, 205152 (2016), arXiv:1606.03724.
- ⁴³D. Xiao, M.-C. Chang, and Q. Niu, “Berry phase effects on electronic properties,” *Rev. Mod. Phys.* **82**, 1959–2007 (2010).
- ⁴⁴X. Wan, A. M. Turner, A. Vishwanath, and S. Y. Savrasov, “Topological semimetal and Fermi-arc surface states in the electronic structure of pyrochlore iridates,” *Phys. Rev. B* **83**, 205101 (2011).
- ⁴⁵H. Yang, Y. Sun, Y. Zhang, W.-J. Shi, S. S. P. Parkin, and B. Yan, “Topological Weyl semimetals in the chiral antiferromagnetic materials Mn₃Ge and Mn₃Sn,” arXiv:1608.03404 (2016).
- ⁴⁶Z. Wang, M. G. Vergniory, S. Kushwaha, M. Hirschberger, E. V. Chulkov, A. Ernst, N. P. Ong, R. J. Cava, and B. A. Bernevig, “Time-Reversal-Breaking Weyl Fermions in Magnetic Heusler Alloys,” *Phys. Rev. Lett.* **117**, 236401 (2016), arXiv:1603.00479.
- ⁴⁷A. B. Sushkov, J. B. Hofmann, G. S. Jenkins, J. Ishikawa, S. Nakatsuji, S. Das Sarma, and H. D. Drew, “Optical evidence for a Weyl semimetal state in pyrochlore Eu₂Ir₂O₇,” *Phys. Rev. B - Condens. Matter Mater. Phys.* **92**, 241108(R) (2015), arXiv:1507.01038.
- ⁴⁸B. Yan and C. Felser, “Topological Materials: Weyl Semimetals,” *Annu. Rev. Condens. Matter Phys.* **8**, 337–354 (2017), arXiv:1611.04182.

- ⁴⁹S. Borisenko, D. Evtushinsky, Q. Gibson, A. Yaresko, T. Kim, M. N. Ali, B. Buechner, M. Hoesch, and R. J. Cava, “Time-Reversal Symmetry Breaking Type-II Weyl State in YbMnBi₂,” arXiv: (2015), 10.1017/CBO9781107415324.004, arXiv:1507.04847.
- ⁵⁰M. Chinotti, A. Pal, W. J. Ren, C. Petrovic, and L. Degiorgi, “Electrodynamical response of the type-II Weyl semimetal YbMnBi₂,” *Phys. Rev. B* **94**, 245101 (2016).
- ⁵¹A. Wang, I. Zaliznyak, W. Ren, L. Wu, D. Graf, and V. O. Garlea, “Magnetotransport study of Dirac fermions in YbMnBi₂ antiferromagnet,” **94**, 165161 (2016).
- ⁵²D. Chaudhuri, B. Cheng, A. Yaresko, Q. D. Gibson, R. J. Cava, and N. P. Armitage, “An optical investigation of the strong spin-orbital coupled magnetic semimetal YbMnBi₂,” arXiv:1701.08693v1.
- ⁵³Y. Zhang, Y. Sun, H. Yang, J. Železný, S. P. P. Parkin, C. Felser, and B. Yan, “Strong anisotropic anomalous Hall effect and spin Hall effect in the chiral antiferromagnetic compounds Mn₃X (X= Ge, Sn, Ga, Ir, Rh and Pt),” *Phys. Rev. B* **95**, 075128 (2017).
- ⁵⁴N. Kiyohara, T. Tomita, and S. Nakatsuji, “Giant Anomalous Hall Effect in the Chiral Antiferromagnet Mn₃Ge,” *Phys. Rev. Appl.* **5**, 064009 (2016), arXiv:1511.04619.
- ⁵⁵J. Sinova, S. O. Valenzuela, J. Wunderlich, C. H. Back, and T. Jungwirth, “Spin Hall effects,” *Rev. Mod. Phys.* **87**, 1213–1260 (2015), arXiv:1411.3249.
- ⁵⁶H. Chen, Q. Niu, and A. H. MacDonald, “Anomalous Hall Effect Arising from Noncollinear Antiferromagnetism,” *Phys. Rev. Lett.* **112**, 017205 (2014).
- ⁵⁷J. Kübler and C. Felser, “Non-collinear antiferromagnets and the anomalous Hall effect,” *Europhys. Lett.* **108**, 67001 (2014), arXiv:1410.5985.
- ⁵⁸F. D. M. Haldane, “Model for a Quantum Hall Effect without Landau Levels: Condensed-Matter Realization of the {‘Parity Anomaly’},” *Phys. Rev. Lett.* **61**, 2015 (1988).
- ⁵⁹R. Shindou and N. Nagaosa, “Orbital Ferromagnetism and Anomalous Hall Effect in Antiferromagnets on the Distorted fcc Lattice,” *Phys. Rev. Lett.* **87**, 116801 (2001).
- ⁶⁰T. Tomizawa and H. Kontani, “Anomalous Hall effect in the t_{2g} orbital kagome lattice due to noncollinearity: Significance of the orbital Aharonov-Bohm effect,” *Phys. Rev. B* **80**, 100401(R) (2009); “Anomalous Hall effect due to noncollinearity in pyrochlore compounds: Role of orbital Aharonov-Bohm effect,” *Phys. Rev. B* **82**, 104412 (2010).
- ⁶¹A. A. Burkov and L. Balents, “Weyl Semimetal in a Topological Insulator Multilayer,” *Phys. Rev. B* **107**, 127205 (2011); K. Y. Yang, Y. M. Lu, and Y. Ran, “Quantum Hall effects in a Weyl semimetal: Possible application in pyrochlore iridates,” *Phys. Rev. B* **84**, 075129 (2011), arXiv:1105.2353.
- ⁶²S. Nakatsuji, N. Kiyohara, and T. Higo, “Large anomalous Hall effect in a non-collinear antiferromagnet at room temperature,” *Nature* **527**, 212–216 (2015).
- ⁶³A. K. Nayak, J. E. Fischer, Y. Sun, B. Yan, J. Karel, A. C. Komarek, C. Shekhar, N. Kumar, W. Schnelle, J. Kübler, C. Felser, S. S. P. Parkin, J. Kübler, C. Felser, and S. S. P. Parkin, “Large anomalous Hall effect driven by a nonvanishing Berry curvature in the noncollinear antiferromagnet Mn₃Ge,” *Sci. Adv.* **2**, e1501870–e1501870 (2016), arXiv:1511.03128.
- ⁶⁴T. Suzuki, R. Chisnell, A. Devarakonda, Y.-T. Liu, W. Feng, D. Xiao, J. W. Lynn, and J. G. Checkelsky, “Large anomalous Hall effect in a half-Heusler antiferromagnet,” *Nat. Phys.* **12**, 1119 (2016).
- ⁶⁵P. Zhou, C. Q. Sun, and L. Z. Sun, “Two Dimensional Antiferromagnetic Chern Insulator: NiRuCl₆,” *Nano Lett.* **16**, 6325–6330 (2016), arXiv:1601.07705.
- ⁶⁶X.-Y. Dong, S. Kanungo, B. Yan, and C.-X. Liu, “Time-reversal-breaking topological phases in antiferromagnetic Sr₂FeOsO₆ films,” *Phys. Rev. B* **94**, 245135 (2016).
- ⁶⁷J.-P. Hanke, F. Freimuth, C. Niu, S. Blügel, and Y. Mokrousov, “Mixed Weyl semimetals and dissipationless magnetization control in insulators,” arxiv.org/1701.08050 (2017), arXiv:1701.08050.
- ⁶⁸F.-Y. Li, Y.-D. Li, Y. B. Kim, L. Balents, Y. Yu, and G. Chen, “Weyl magnons in breathing pyrochlore antiferromagnets,” *Nat. Commun.* **7**, 12691 (2016), arXiv:1602.04288.
- ⁶⁹N. Kanazawa, Y. Onose, T. Arima, D. Okuyama, K. Ohoyama, S. Wakimoto, K. Kakurai, S. Ishiwata, and Y. Tokura, “Large Topological Hall Effect in a Short-Period Helimagnet MnGe,” *Phys. Rev. Lett.* **106**, 156603 (2011).
- ⁷⁰M. Hoffmann, J. Weischenberg, B. Dupé, F. Freimuth, P. Ferriani, Y. Mokrousov, and S. Heinze, “Topological orbital magnetization and emergent Hall effect of an atomic-scale spin lattice at a surface,” *Phys. Rev. B* **92**, 020401 (2015), arXiv:1503.01885v2.
- ⁷¹Y. Machida, S. Nakatsuji, S. Onoda, T. Tayama, and T. Sakakibara, “Time-reversal symmetry breaking and spontaneous Hall effect without magnetic dipole order,” *Nature* **463**, 210–213 (2010).
- ⁷²C. Sürgers, G. Fischer, P. Winkel, and H. V. Löhneysen, “Large topological Hall effect in the non-collinear phase of an antiferromagnet,” *Nat. Commun.* **5**, 3400 (2014).
- ⁷³C. Sürgers, W. Kitzler, T. Wolf, and H. v. Löhneysen, “Anomalous Hall effect in the noncollinear antiferromagnet

- Mn₅Si₃,” AIP Adv. **6**, 055604 (2016), arXiv:1601.01840.
- ⁷⁴J. Zhou, Q. F. Liang, H. Weng, Y. B. Chen, S. H. Yao, Y. F. Chen, J. Dong, and G. Y. Guo, “Predicted Quantum Topological Hall Effect and Noncoplanar Antiferromagnetism in K_{0.5}RhO₂,” Phys. Rev. Lett. **116**, 256601 (2016), arXiv:1602.08553.
- ⁷⁵Y. Sun, Y. Zhang, C. Felser, and B. Yan, “Strong Intrinsic Spin Hall Effect in the TaAs Family of Weyl Semimetals,” Phys. Rev. Lett. **117**, 146403 (2016), arXiv:1604.07167.
- ⁷⁶G. Yin, Y. Liu, Y. Barlas, J. Zang, and R. K. Lake, “Topological spin Hall effect resulting from magnetic skyrmions,” Phys. Rev. B **92**, 024411 (2015), arXiv:1503.00242.
- ⁷⁷Y. Zhang, J. Zelezny, Y. Sun, J. van den Brink, and B. Yan, “Spin Hall effect emerging from a chiral magnetic lattice without spin-orbit coupling,” Arxiv Prepr. (2017), arXiv:1704.03917.
- ⁷⁸J. P. Hanke, F. Freimuth, A. K. Nandy, H. Zhang, S. Blügel, and Y. Mokrousov, “Role of Berry phase theory for describing orbital magnetism: From magnetic heterostructures to topological orbital ferromagnets,” Phys. Rev. B **94**, 121114(R) (2016), arXiv:1603.07683.
- ⁷⁹J.-P. Hanke, F. Freimuth, S. Blügel, and Y. Mokrousov, “Prototypical topological orbital ferromagnet γ -FeMn,” Sci. Rep. **7**, 41078 (2017).
- ⁸⁰P. M. Buhl, F. Freimuth, S. Blügel, and Y. Mokrousov, “Topological spin Hall effect in antiferromagnetic skyrmions,” Phys. status solidi - Rapid Res. Lett. **11**, 1700007 (2017).
- ⁸¹C. Jin, C. Song, J. Wang, and Q. Liu, “Dynamics of antiferromagnetic skyrmion driven by the spin Hall effect,” Appl. Phys. Lett. **109**, 182404 (2016).
- ⁸²G. Finocchio, F. Büttner, R. Tomasello, M. Carpentieri, and M. Kläui, “Magnetic skyrmions: from fundamental to applications,” J. Phys. D: Appl. Phys. **49**, 423001 (2016).
- ⁸³Z. Liu and H. Ian, “Numerical studies on antiferromagnetic skyrmions in nanodisks by means of a new quantum simulation approach,” Chem. Phys. Lett. **649**, 135–140 (2016), arXiv:1601.05170v1.
- ⁸⁴S. Rohart, J. Miltat, and A. Thiaville, “Path to collapse for an isolated Néel skyrmion,” Phys. Rev. B **93**, 214412 (2016).
- ⁸⁵A. N. Bogdanov, U. K. Roessler, M. Wolf, and K. H. Müller, “Magnetic structures and reorientation transitions in noncentrosymmetric uniaxial antiferromagnets,” Phys. Rev. B **66**, 214410 (2002), arXiv:0206291 [cond-mat].
- ⁸⁶T. Morinari, “Half-Skyrmion Theory for High-Temperature Superconductivity,” in *The Multifaceted Skyrmion* (World Scientific, 2010) pp. 311–331.
- ⁸⁷X. Zhang, Y. Zhou, and M. Ezawa, “Antiferromagnetic Skyrmion: Stability, Creation and Manipulation,” Sci. Rep. **6**, 24795 (2016), arXiv:1504.01198.
- ⁸⁸J. Barker and O. A. Tretiakov, “Static and Dynamical Properties of Antiferromagnetic Skyrmions in the Presence of Applied Current and Temperature,” Phys. Rev. Lett. **116**, 147203 (2016).
- ⁸⁹H. Velkov, O. Gomonay, M. Beens, G. Schwiete, A. Brataas, J. Sinova, and R. A. Duine, “Phenomenology of current-induced skyrmion motion in antiferromagnets,” New J. Phys. **18**, 075016 (2016), arXiv:1604.05712.
- ⁹⁰X. Zhang, Y. Zhou, and M. Ezawa, “Magnetic bilayer-skyrmions without skyrmion Hall effect,” Arxiv Prepr. **7**, 1504.02252 (2015), arXiv:1504.02252.
- ⁹¹S. Zhang, A. A. Baker, S. Komineas, and T. Hesjedal, “Topological computation based on direct magnetic logic communication,” Sci. Rep. **5**, 15773 (2015).
- ⁹²Q. L. He, G. Yin, L. Yu, A. J. Grutter, L. Pan, X. Kou, X. Che, G. Yu, T. Nie, B. Zhang, Q. Shao, K. Murata, X. Zhu, Y. Fan, X. Han, B. J. Kirby, and K. L. Wang, “Topological transitions induced by antiferromagnetism in a thin-film topological insulator,” Arxiv Prepr. (2016), arXiv:1612.01661.
- ⁹³S. Ghosh and A. Manchon, “Spin-orbit torque in two-dimensional antiferromagnetic topological insulators,” Phys. Rev. B **95**, 035422 (2017).
- ⁹⁴A. Kandala, A. Richardella, S. Kempinger, C.-X. Liu, and N. Samarth, “Giant anisotropic magnetoresistance in a quantum anomalous Hall insulator,” Nat. Commun. **6**, 7434 (2015), arXiv:1503.0355.
- ⁹⁵C. Carbone, P. Moras, P. M. Sheverdyaeva, D. Pacile, M. Papagno, L. Ferrari, D. Topwal, E. Vescovo, G. Bihlmayer, F. Freimuth, Y. Mokrousov, and S. Blügel, “Asymmetric band gaps in a Rashba film system,” Phys. Rev. B - Condens. Matter Mater. Phys. **93**, 125409 (2016).
- ⁹⁶Q.-K. Xue, “Nanoelectronics: A topological twist for transistors,” Nat. Nanotechnol. **6**, 197–198 (2011).
- ⁹⁷J. Liu, T. H. Hsieh, P. Wei, W. Duan, J. Moodera, and L. Fu, “Spin-filtered Edge States with an Electrically Tunable Gap in a Two-Dimensional Topological Crystalline Insulator,” Nat. Mater. **13**, 178–183 (2013), arXiv:1310.1044.
- ⁹⁸H. Fujita, “Field-free, spin-current control of magnetization in non-collinear chiral antiferromagnets,” Phys. status solidi - Rapid Res. Lett. (2016), 10.1002/pssr.201600360, arXiv:1610.07615.
- ⁹⁹W. Feng, G.-Y. Guo, J. Zhou, Y. Yao, and Q. Niu, “Large magneto-optical Kerr effect in noncollinear antiferromagnets Mn₃X (X = Rh, Ir, Pt),” Phys. Rev. B **92**, 144426 (2015).
- ¹⁰⁰D. Thouless, *Topological Quantum Numbers in Nonrelativistic Physics* (World Scientific, 1998).